Membrane dynamics promote sensitivity of epithelial cancer targets to pro-necrotic activity of Natural Killer cells

Yanting Zhu[1], Jun Xie[1] and Jue Shi[1*]

[1] Center for Quantitative Systems Biology, Department of Physics and Department of Biology, Hong Kong Baptist University, Hong Kong, China

* Corresponding author: Jue Shi, jshi@hkbu.edu.hk

Keywords: NK cell cytotoxicity; Target variability; Membrane dynamics; Single cell dynamics; necrosis

Abstract

Natural Killer (NK) cells play a key role in eliminating virus-infected cells and cancer cells. Although molecular machineries mediating their activity and specificity have been extensively studied, our understanding of the determinants that govern the differential cytotoxicity of NK cells against distinct epithelial cell targets is still limited. By employing a live-cell FRET reporter and quantitative single cell imaging, we characterized the dynamic phenotypes and rate-limiting kinetics of a panel of normal and epithelial cancer cells to killing by primary human NK cells. We uncovered intriguing target-dependent variability in their sensitivity to three distinct NK cell cytotoxic modes mediated by granzyme, death ligand and the largely unexplored necrosis. While NK-target cell interaction via known inhibitory and activating receptors, in particular the KIRs, largely determined the overall cytotoxic activity, we found the variable sensitivity to distinct NK cell cytotoxic modes was not regulated by individual receptors. Instead, plasma membrane dynamics driven by blebs and/or lamellipodia appeared to control the induction of different cytotoxic modes in a target-specific manner, particularly promoting necrotic killing. Our results point to modulating the membrane dynamics of epithelial cell targets as a viable strategy to control the degree, timing and inflammatory consequences of NK cell killing.

Introduction

Natural Killer (NK) cells detect and kill abnormal cell targets, and are considered a promising immunotherapeutic candidate [1, 2]. Harnessing and stimulating the direct cytotoxic activity of NK cells has attracted growing interest in the recent development of cancer immunotherapy, as diverse tumor cell types showed susceptibility to NK cell killing and targeted therapy and immune checkpoint therapy may also act in part via triggering NK cell response [3-5]. Tumors are known to harbor large genetic and phenotypic heterogeneity that likely impact their differential interactions with NK cells. However, the mechanistic basis underlying the dynamic control over NK cells' selective killing of distinct target cell types, e.g., normal vs. cancer as well as different types of cancer, such as those with hot vs. cold inflammatory microenvironment, is poorly understood.

NK cells are known to detect abnormal cells by integrating signals from various inhibitory and activating receptors on their cell surfaces [6, 7]. The major inhibitory receptors on NK cells are killer cell immunoglobulin-like receptors (KIRs), which interact with major histocompatibility complex I (MHCI) molecules of the target cells, leading to NK cell "self-tolerance" but activation when encountering "foreign" or transformed targets, such as tumor cells with low MHCI expression. Among the many different NK cell activating receptors, NKG2D has been particularly implicated in NK cell-mediated immunity against tumors [8]. Ligands for NKG2D, such as MICA (MHC class I-related gene A), MICB (MHC class I-related gene B) and ULBP (UL16-binding protein), are expressed in most human tumors [9], and inhibiting NKG2D function attenuated NK cell cytotoxicity against tumor targets [10]. However, the determinants of overall selectivity of NK cells towards particular cancer cell type in terms of both the extent of cytotoxic response as well as cytotoxic mechanism is still poorly understood. And so far the field has very much focused on molecular determinants, while ignoring possible physical and mechanical determinants.

Upon recognition of abnormal cell targets, NK cells can elicit direct target cell death by

three main mechanisms, i.e., lytic granule-mediated apoptosis, death ligand-mediated apoptosis and necrosis [11-13]. Lytic granule-mediated cytotoxicity is considered the principal cytotoxic pathway of NK cells. Upon formation of NK-target cell immunological synapses, lytic granules release perforin and granzymes into the synapse. Granzymes enter the target cell via perforin channels, where they activate the apoptosis pathway via proteolytic activation of caspases [14]. In addition, NK cells express a variety of death ligands, such as Fas ligand (FasL) and TNF-related apoptosis inducing ligand (TRAIL), which engage cognate death receptors expressed on the target cell surface, triggering death by receptor-mediated extrinsic apoptosis [15, 16]. Target cell death by NK cell-induced necrosis has only been reported in a few studies and its mechanistic basis is still largely unknown [13, 17].

To unravel the target specificity of NK cell cytotoxicity, in this study we characterized the rate-limiting kinetics and phenotypic heterogeneity of NK cell cytotoxic activity against normal and a variety of epithelial cancer cell targets using quantitative single cell microscopy assays. And we pinpointed the dynamic control over the target dependence of NK cell cytotoxic activity and cytotoxic mechanism. Intriguingly, we found the variable sensitivity of epithelial target cells to overall NK killing was conferred mainly by the inhibitory NK cell ligand, MHCI, but not the various activating NK cell ligands, and the target selectivity of NK cell cytotoxic mechanism, e.g., necrosis vs. apoptosis, was determined by differential plasma membrane dynamics of the epithelial cell targets, instead of the well-known inhibitory/activating signaling machinery.

Results

Target cell type dependence of NK cell cytotoxic dynamics

To investigate mechanisms that underlie target preferences of NK cells, we chose a panel of mammalian epithelial cell lines that exhibited variable sensitivity to primary NK cell killing, including one normal cell line, LO2 (immortalized normal hepatic cell line) and four cancer cell lines, i.e., HeLa (cervix cancer), SMMC-7721 (liver cancer), MCF7 (breast cancer), and U-2 OS (bone cancer). To visualize dynamic response to NK cells, we engineered each epithelial cell line with a fluorescent reporter of granzyme-B activity (GzmB-FRET) as well as a mitochondria reporter of apoptosis (IMS-RP), as reported previously [18-20]. All NK-target cell co-culture assays were conducted with human primary NK cells purified from healthy blood donors and pre-activated by IL-2 for three days, at an NK-to-target cell ratio of 3:1. Target cell death was scored morphologically by blebbing followed by cell lysis, and the time from NK cell addition to morphological target cell death was plotted as cumulative survival curves. As shown in Figure 1A, the normal cell line, LO2, was the most resistant to NK cell killing, consistent with NK cell's function in eliminating abnormal and cancerous cells. Among the cancer cell lines, SMMC-7721 and MCF7 were the most sensitive, with MCF7 exhibiting the fastest kinetics to cell death.

In addition to variable sensitivity of the epithelial cell lines to overall NK cell killing, we also observed striking difference in their susceptibility to distinct cytotoxic modes of NK cells. The majority of cell death (about 60%) seen in SMMC-7721 were preceded by a loss of the granzyme-B FRET (i.e., an increase of CFP (donor) signal and decrease of YFP (acceptor) signal) followed by mitochondrial outer membrane permeabilization (MOMP), suggesting that NK cells killed SMMC-7721 mainly by the lytic granule cytotoxic pathway and intrinsic apoptosis (Fig. 1B). In contrast, NK cell cytotoxicity towards U-2 OS cells mostly did not associate with change in the granzyme-B FRET signal. We have previously characterized this mode of target cell death to be mediated by the death ligand, e.g., FasL, and subsequent

extrinsic apoptosis [19]. Intriguingly, we found necrosis, a largely unexplored NK cell cytotoxic mechanism, was the primary cytotoxic mode to trigger cell death in MCF7 cells. As shown in the bottom panel of Figure 1B, MCF7 cell death was not preceded by MOMP, indicating it was not classic apoptosis. Moreover, signal from the granzyme-B FRET reporter was abruptly lost upon extensive MCF7 cell blebbing, pointing to large scale leakage of the intracellular content likely due to membrane ruptures. Such dynamic features were consistent with necrotic cell death.

Figure 1C summarized the percentage of live target cells and the cell death population via the three distinct cytotoxic modes of primary NK cell exhibited by the five epithelial target cell lines, including lytic granule-mediated apoptosis, death ligand-mediated apoptosis and necrosis after 12 hours of NK-target cell co-culture. The two most sensitive target cell lines, SMMC-7721 and MCF7, which showed rapid kinetics of cell death induction, were killed mainly (around 60%) through granzyme B activity or necrosis, while cytotoxicity mediated by death ligand was more dominant in the less sensitive target cell types, U-2 OS, HeLa and LO2. All target cell lines showed substantial cell death triggered by death ligands of NK cells, ranging from 23% to 57% of the total target cell population, suggesting the death receptor pathway is widespread. In contrast, the extent of cell death activated by the lytic granule and necrosis pathways varied more significantly, ranging from 1% to 54% for the lytic granule mode and 1% to 57% for the necrotic mode. Such large variability in the sensitivity to NK cell killing via lytic granule and necrosis indicated that activation of these two cytotoxic modes may depend on epithelial features that are more cell type specific.

Extent of cytotoxicity, but not cytotoxic mode, correlated with MHCI expression

To investigate the potential molecular determinants underlying the observed variable sensitivity of epithelial cell lines to overall NK cell killing as well as to the distinct NK cell cytotoxic modes, we first profiled the expressions of NK cell-interacting surface molecules

known to be involved in activating NK cell cytotoxicity for the target cell panel. These molecules include the human MHCI molecule (HLA-A,B,C), NKG2D ligands (MICA, MICB and ULBP-2,5,6) and DNAM-1 ligands (PVR/CD155 and Nectin-2/CD112) [21]. We also measured the expression of the death receptor Fas and an integrin key for NK cell adhesion, ICAM-1 (CD54), in our analysis by flow cytometry (Fig. 2A).

The quantified FACS results showed highly variable expressions of all surface molecules that we profiled between the five target cell lines (Fig. 2B). The sensitivity of target cell lines to overall NK cell killing correlated relatively well with the expression level of the inhibitory MHCI molecules, and to a much lesser extent with MICB, but did not correlate with the expression of the other NKG2D activating ligands, MICA and ULBPs, or the activating ligands for DNAM-1. Surprisingly, the expression level of Fas did not correlate with the differential sensitivity to the death ligand-mediated NK cell cytotoxicity. Our data thus indicated that the inhibitory strength of KIRs-MHCI may exert the primary control over target cell recognition and overall NK cell cytotoxicity against a particular epithelial target, while control by the activating ligands is less universal and more context-dependent. However, our data did not show any significant correlative feature that was specific to the three distinct NK cell cytotoxic modes. The only differential ligand expression that may potentially render specificity to necrotic killing is MICB, as the MICB expression level in MCF7, the cell line that was particularly prone to necrotic death, was 5-10 folds higher than that in the other four cell lines. However, RNAi knockdown of MICB in MCF7 cells did not attenuate necrotic death induced by NK cells, indicating MICB expression was not the molecular determinant for the activation of necrotic killing by NK cells (data not shown).

Target dependence of NK cell cytotoxicity on inhibitory and activating receptors

As we did not observe correlation between the expression of well-known NK cell-interacting surface ligands with the sensitivity of different target cell lines to distinct NK

cell cytotoxic modes, we next investigated the functional involvement of the key inhibitory and activating receptors on NK cell surface, as the target specificity could be conferred by surface ligands not in the profiling panel as discussed above. The NK cell receptors that we examined included two types of inhibitory receptors, KIRs and NKG2A (CD94), and three activating receptors important for cancer target recognition, including NKG2D (CD314), DNAM-1 (CD226) and NKp46 (CD335) [11, 21]. Specifically, we used neutralizing antibodies to block individual receptors or combination of the receptors and then compared the extent and kinetics of target cell death via the three cytotoxic modes with those under the control condition (i.e., no receptor blocking). As there are several KIRs that recognize different HLA molecules on the target cell surface, we used a broad-spectrum neutralizing antibody against HLA-A, -B and -C to block the interaction of all KIRs and human MHCI molecules as a whole, instead of examining the individual KIR, to simplify the analysis.

Figure 3A and 3B showed the receptor neutralizing results for HeLa cells in co-culture with primary NK cells. As expected, blocking the inhibitory NK-HeLa cell interaction via MHCI molecules or NKG2A accelerated and enhanced HeLa cell killing, with MHCI neutralization showing a stronger effect (Fig. 3A). Moreover, simultaneous blockage of MHCI molecules and NKG2A further increased NK cell cytotoxicity towards HeLa, resulting in a degree of cell death similar to that observed in the sensitive target cell lines, such as SMMC-7721. In contrast, neutralizing the activating receptors exerted less prominent effect in attenuating the cell death response of HeLa, possibly because HeLa cells under the control condition (i.e., no receptor blocking) were already relatively resistant to primary NK cell killing. Inhibition of NKG2D activity exhibited a stronger effect in attenuating cell death than neutralizing DNAM-1 or NKp46 (Fig. 3A). Double blocking of NKG2D plus DNAM-1 or NKp46 further rescued HeLa cell death, confirming that the NK cell cytotoxicity is regulated by collective, rather than individual, signaling receptors.

We next investigated how blocking individual receptors altered induction of the three

cytotoxic modes, expecting individual receptors to selectively regulate particular modes. However, this was not the result. The fraction of NK cell killing mediated by lytic granule, death ligand and necrosis all increased in parallel upon blockage of the inhibitory KIR-MHCI interaction, and decreased in parallel upon neutralizing the activating receptor NKG2D, either alone or in combination with DNAM-1 or NKp46 (except for the necrotic population under NKG2D+ NKp46 inhibition). This parallel activation or inhibition of all three pathways can be seen by the same relative height of the three non-white bars in Figure 3B, noting that relative heights were less accurate when overall killing was low. Therefore, in HeLa, receptor modulation appears to tune the overall cytotoxic activity of NK cells and/or receptivity of targets, but not the precise death pathway.

Figure 3C summarized the receptor neutralization results for all three pathways across the five epithelial target cell lines. Here, we plotted the ratio of perturbation versus control. Intuitively, data points along the diagonal indicated no change relative to the control condition, and the further away the data points were from the diagonal, the larger the effect of the respective receptor inhibition in diverting the cell death response into, or away from, one of the three cytotoxic modes. Similar to HeLa cells, neutralization of the inhibitory KIRs-MHCI interaction exerted strong effect in enhancing cell death response of the other four target cell lines, and loss of NKG2D activity exerted the strongest effect in attenuating target cell death. Double inhibition of NKG2D and DNAM-1 nearly abrogated cell death of U-2 OS, SMMC-7721 and MCF7, the three cell lines that were most sensitive to NK cell killing. However, as of HeLa cells, the three cytotoxic modes were altered approximately in parallel, again showing that receptor modulation tuned overall activity of NK cells much more than activity of one specific death pathway. We also noted that except for MCF7, no other cell line showed significant cell death via necrosis under all receptor perturbation conditions, suggesting that MCF7 cells may have unique cellular features that promote the induction of necrotic killing, which we further examined below.

Membrane dynamics modulate target sensitivity to distinct NK cell cytotoxic modes

Since receptor expression level did not predict which death pathway is preferred, and receptor inhibition did not modulate the fraction of death caused by particular pathway, we sought other phenotypic properties that might predict and modulate individual NK cell cytotoxic pathways. We focused on MCF7 and SMMC-7721 because they had the most distinctive preferences, i.e., MCF7 cells were uniquely sensitive to necrosis, while SMMC-7721 cells were sensitive to lytic granule-mediated intrinsic apoptosis. A distinguishing feature of these cell lines in our movies was differences in plasma membrane dynamics. MCF7 cells exhibited extensive dynamic protrusions driven by membrane blebs and lamellipodia (Fig. 4A). In contrast, SMMC-7721 cells exhibited only moderate membrane dynamics and the membrane of U-2 OS cells was largely quiet (Fig. 4A). This observation led us to examine whether differential membrane dynamics of the epithelial cell targets contributed to the activation of distinct cytotoxic modes.

To attenuate the formation of dynamic membrane protrusions, we used either NSC23766, an inhibitor of the small GTPase Rac1, to inhibit actin polymerization-driven lamellipodia, or Y27632, an inhibitor of the Rho Kinase (ROCK), to inhibit contractility-driven membrane blebs [22-24]. NSC23766 significantly reduced membrane protrusions in both MCF7 and SMMC-7721 cells, as evidenced by the kymograph of cell edge, which showed a relatively smooth edge under NSC23766 as compared to a jagged edge in the control cells (Fig. 4A). The effect of Y27632, however, diverged in MCF7 and SMMC-7721. MCF7 cells treated with Y27632 showed reduced membrane blebs but longer lamellipodia, a phenotype previously characterized as due to compensatory effects of membrane blebs and lamellipodia [22]. SMMC-7721 treated with Y27632 showed reduced protrusions, but small ruffles remained. Attenuation of membrane dynamics by both NSC23766 and Y27632 changed the primary cell death mode of MCF7 cells from necrosis to death ligand-mediated apoptosis, with NSC23766 exhibiting a slightly stronger effect (Fig.

4B). NSC23766 treatment of SMMC-7721 also resulted in a switch of NK cell killing from lytic granule-mediated apoptosis to death ligand-mediated apoptosis, while Y27632 did not show significant effect on altering the NK cell cytotoxic mode (Fig. 4C). Our data thus showed inhibiting plasma membrane dynamics of epithelial targets promoted NK cell killing via death ligand-mediated apoptosis, while damping the other two cytotoxic modes.

Next we examined whether increasing membrane dynamics, e.g., in SMMC-7721, would alter NK cell killing from lytic granule-mediated apoptosis to the necrosis mode, similar to MCF7 cells. We noted that SMMC-7721 cells showed extensive membrane blebs when they started to adhere to the cell culture plate surface (Fig. 4D, left panel). And these blebs disappeared upon complete adherence (Fig. 4A, control). We thus co-cultured primary NK cells with SMMC-7721 that were trypsinized and seeded onto the culture plate for only 4 hours to investigate the effect of enhanced membrane dynamics, in this case, driven by blebs, on NK cell killing mode. Compared to control SMMC-7721 cells that had adhered to the culture plate for 24 hours, which were mainly (~60%) killed by lytic granule-mediated apoptosis, the majority (~50%) of the short-adherence cells were killed via the necrotic mode (Fig. 4D, right panel). And addition of the bleb inhibitor, Y27632, abrogated the increase in necrotic killing of the short-adherence cells (Fig. 4D). As U-2 OS cells adhered to the culture plate surface very quickly (about 3-5 hours) and did not exhibit prolonged blebs, we were unable to use this experimental strategy to study the effect of enhanced membrane dynamics on promoting lytic granule-mediated apoptosis over the death ligand-mediated mode. Nonetheless, overall our results suggested that the extent of membrane dynamics exerted a key control over the sensitivity of different epithelial targets to the three distinct NK cell cytotoxic modes.

As necrotic death is associated with membrane rupture, we hypothesized that membrane pores formed by perforin at the NK-target cell conjugation may be involved in triggering the membrane rupture and subsequent necrosis. Moreover, it is possible that a highly dynamic

membrane, e.g., in MCF7 cells, facilitated excessive lytic granule transfer, thus resulting in large perforin pores that induced necrotic membrane rupture rather than the more controlled apoptosis catalyzed by granzyme-B. To test the role of lytic granule and perforin in the necrotic mode of NK cell cytotoxicity, we pre-treated primary NK cells with Concanamycin A (CMA), an inhibitor of vacuolar type ATPase (V-ATPase) that attenuated lytic granule transfer, and then co-cultured NK cells with MCF7 cells. As shown in Figure 4E, 10 nM CMA was sufficient to reduce necrotic killing of MCF7 cells from 53% to 4% after 12 hours of co-culture as well as abrogating lytic granule-mediated apoptosis, confirming the key role of lytic granule transfer and likely perforin in mediating these two cytotoxic pathways. The extent of death ligand-mediated apoptosis was not affected by CMA treatment, pointing to no interdependence between the different cytotoxic modes. Moreover, we found that intermediate dosage of CMA, i.e., 4-5 nM, partially reduced necrotic death in MCF7 cells to about 25%. Interestingly, the decrease in necrotic killing at intermediate CMA concentrations was accompanied by an increase of lytic granule-mediated apoptosis (from 8% to 20%), suggesting that attenuation of lytic granule transfer and possibly the resulting smaller membrane pores may shift necrotic killing to the less inflammatory granzyme-B mediated apoptosis.

Discussion

Our study revealed epithelial cell targets varied not only in their overall sensitivity to primary NK cell killing but also to distinct NK cell cytotoxic modes, providing a new angle to modulate the kinetics and inflammatory consequences of NK cell cytotoxic activity. Target specificity to distinct NK cell cytotoxic modes was found to be not determined by the inhibitory/activating receptor machinery, and exhibited rather constant ratios between modes when overall killing was tuned in both directions. A novel determinant of killing mode identified from our work was the extent of plasma membrane dynamics of the epithelial cell targets. A highly dynamic membrane driven by blebs and/or lamellipodia correlated with mostly necrotic killing in MCF7 cells, though we also noted that the loss of caspase-3 in MCF7 may also contribute to its resistance to the intrinsic apoptosis pathway [25]. In contrast, the lytic granule-mediated and death ligand-mediated cytotoxicity are induced in response to moderate and low membrane dynamics of the target cells. We previously showed the death ligand-mediated killing mode induced more gradual target cell death than the lytic granule mode [19]. Hence, inhibiting/activating membrane dynamics that alter the cytotoxic modes could potentially tune the kinetics and extent of cytotoxic response to NK cells. Moreover, as necrotic death releases cell debris to “inflame” the local microenvironment, altering the NK cell cytotoxic modes, i.e., necrosis vs. apoptosis, by modulating target membrane dynamics can enhance or damp the secondary inflammatory response subsequent to NK cell killing. This may hold the potential of, e.g., amplifying the anti-tumor effect of adoptive cell transfer therapy beyond primary NK cell killing.

The Rho family of GTPases, e.g., Rac1 and the associated kinases, e.g., ROCK, are involved in key oncogenic signaling pathways, particularly by activating the actomyosin network and promoting cancer invasion and metastasis [26, 27]. Up-regulation of Rac1 activity has been frequently observed in human cancer [28] and Rac1 inhibitor, such as NSC23766 that we used in this study, is being actively pursued as anticancer therapeutic. Our

data showed that tuning membrane dynamics by targeting Rac1 and ROCK is an effective strategy to influence the cytotoxic mechanism of NK cells. For cancers with elevated activity of Rac1 and/or Rho/ROCK signaling, they are likely more sensitive to inflammatory killing by NK cells via necrosis. And more controlled, apoptotic killing of NK cells can be achieved by combining with Rac1/ROCK inhibitor. As oncogenic activation of receptor tyrosine kinases (RTKs) and Ras signaling also tends to strongly activate protrusive and contractile membrane activity [29], inhibitors of the RTK signaling pathways that block such membrane dynamics could also be possibly employed to modulate NK cell cytotoxicity.

Dynamics of the actomyocin network upon formation of the NK-target cell immunological synapse have been previously studied, demonstrating its functional importance for mediating lytic granule transfer [30, 31]. What is new and unexpected from our study is that we found the degree of actomyosin dynamics determined the activation of distinct NK cell cytotoxic modes. The more active actomyosin network is, the more likely the epithelial cell targets would trigger NK cell killing via necrosis. A quiet actomyosin network did not significantly attenuate the overall cytotoxic activity of NK cells, but alter the cytotoxic mechanism to a slower mode mediated by death ligands. Although the mechanistic link between the strong actomyosin dynamics and necrotic killing is alluded to by our study, it is not completely solved. Based on the CMA results shown in Figure 4E, we speculate that the strong actin and myosin dynamics promote more extensive lytic granule transfer, subsequently allowing more perforin to form large pores to lyse the cells. However, it is also possible that the strong actomyosin dynamics facilitate the actin cytoskeleton to tear the membrane apart. Further study is needed to distinguish these two scenarios and pinpoint the origin of necrotic cytotoxicity of NK cells.

Previous studies have showed Ca^{2+} played an important role in mediating lytic granule transfer upon NK-target cell interaction. We confirmed that chelating Ca^{2+} by EGTA abrogated both granzyme-B-dependent apoptosis and necrosis induced by primary NK cells

in the cell line panel that we studied (data not shown). However, we did not observe high Ca^{2+} concentration shifted NK cell killing to the necrosis mode, as reported by Backes et al [13]. Increasing Ca^{2+} concentration up to 3.5 mM did not enhance necrotic killing of SMMC-7721 or U-2 OS cells. And Ca^{2+} concentration higher than 3.5 mM triggered cell death in the absence of NK cells, possibly due to the high salt concentration and osmotic stress. As Backes et al used suspension cells as NK cell targets, e.g., Jurkat E6-1 and K562, while we used epithelial targets, the difference between our results regarding the role of Ca^{2+} in necrotic killing may be due to target cell type variation, i.e., suspension vs. adherence, which is of interest for further study.

The fact that we did not observe correlation between the expression levels of the commonly known NK cell activating ligands and the sensitivity of epithelial cell targets to overall NK cell killing re-affirmed the difficulty of developing biomarker from the cancer-associated activating ligands to predict patient prognosis or their response to NK cell therapy. Counter-intuitively, we found the normal cell line, LO2, which was the most resistant to NK cell cytotoxicity, expressed the highest level of NKG2D ligand, MICA, and also high level of ULPs when compared with the cancer cell lines (Fig. 3B). Previous clinical studies have also showed that high levels of NKG2D ligands were not associated with the extent of NK cell infiltration into the tumors or better prognosis for patients with breast, lung or ovarian cancers [32-34], suggesting that expressions of NK cell activating ligands likely vary significantly between cancer types and tumor context, thus hindering their stand-alone prognostic potential.

Materials and Methods

Isolation of primary NK cells from human blood

Primary human NK cells were isolated from fresh human buffy coat (within 24 hours of blood donation) obtained from the Hong Kong Red Cross, by Ficoll-Paque Plus solution and subsequent negative selection of Peripheral Blood Mononuclear Cells (PBMCs) using the EasySep Human NK Cell Enrichment Kit (STEMCELL Technologies), according to manufacturer's protocol. Only NK cell prep with purity higher than 90% (measured by FACS analysis of CD56 staining) was used for experiments. Fresh human NK cells were cultured for 3 days at a density of $1x10^6$ cells/ml in RPMI 1640 medium (Gibco, Thermo Fisher) containing 10 ng/ml recombinant human IL-2 (Gibco, Thermo Fisher), 10% heat-inactivated Fetal Calf Serum (Gibco, Thermo Fisher), 100 U/ml penicillin and 100 μg/ml streptomycin (Gibco, Thermo Fisher), prior to experiments.

Cell lines and cell culture

The live-cell Förster Resonance Energy Transfer (FRET) construct that reports on the granzyme-B proteolytic activity as well as the mitochondrial reporter, IMS-RP, were engineered into the five selected epithelial cell lines by retroviral infection, as described previously [18, 19]. Isogenic clones of the fluorescent reporter cell lines that exhibited cell death response to primary NK cell killing most similar to their respective parental lines were selected for performing the live-cell imaging assays. Cell lines were cultured in appropriate medium supplemented with 10% Fetal Calf Serum, 100 U/ml penicillin and 100 μg/ml streptomycin. Specifically, U-2 OS was maintained in McCoy's 5A (Modified) Medium; MCF7 was maintained in RPMI 1640 Medium; SMMC-7721, HeLa and LO2 were maintained in Dulbecco's modified Eagles Medium (DMEM). For all co-culture experiments with primary NK cells, the NK-to-target cell ratio of 3:1 were used and 50 ng/ml IL-2 was supplemented in the medium.

Chemicals and neutralizing antibodies

The ROCK inhibitor, Y27632, was purchased from Sigma and used at 5 μM. The Rac inhibitor, NSC23766, was from SelleckChem and used at 120 μM for MCF7 and 50 μM for SMMC-7721. Cells were pre-treated with either Y27632 for 1 hour or NSC23766 for 5-12 hours before experiments. The inhibitor of vacuolar type ATPase (V-ATPase), Concanamycin A, was from Santa Cruz Biotechnology. To block the activity of various NK cell receptors, the following neutralizing antibodies from Biolegend were used: Purified anti-human HLA-A,B,C antibody (Clone W6/32), CD94 (Clone DX22,), NKG2D (Clone 1D11), NKp46 (Clone 9E2), and DNAM-1 (Clone 11A8). Except for HLA-A,B,C antibody, which was used at 5 μg/ml, the rest of the antibodies were used at 10 μg/ml.

Time-lapse microscopy and image analysis

Cells were plated in 96-well μ-plate (ibidi), and cultured in CO_2-independent medium (Gibco, Thermo Fisher) supplemented with 10% heat-inactivated FCS, 4 mM L-glutamine, 100 U/ml penicillin and 100 μg/ml streptomycin. Cells were imaged by a Nikon Eclipse TE-2000 inverted microscope enclosed in a humidified chamber maintained at 37°C with a 20X plan Apo objective (NA = 0.95). Images were acquired every 4 minutes and data were viewed and analyzed using the MetaMorph software (Molecular Devices). Target cell death was scored morphologically by blebbing followed by cell lysis, and the time from NK cell addition to morphological target cell death was plotted as cumulative survival curves. The onset of apoptosis is scored by an abrupt transition from punctate to smooth localization of the mitochondria reporter, IMS-RP. The cytotoxic mode mediated by lytic granule and granzyme B was scored based on the granzyme-B FRET reporter. To quantify the time course of the FRET signal, ImageJ was used to segment the individual cells and measure the total intensity of the YFP and CFP signal, respectively.

Flow cytometry analysis of surface ligand and receptor expression

$1x10^6$ epithelial target cells were washed and re-suspended in the cell staining buffer (Biolegend) containing different dye-conjugated primary antibodies at 1 µg/ml or 5 µg/ml for 30 minutes at 4℃. Cells were then washed and stained with the Zombie NIR (cell death marker, Biolegend). The stained cells were analyzed by flow cytometry with a FACSCanto II cytometer (BD Biosciences). Primary antibodies targeting the various surface ligands and receptors as well as the corresponding control include: FITC anti-human HLA-A,B,C (Clone W6/32, Biolegend), FITC anti-human ICAM-1/CD54 (Clone DX2, Biolegend), FITC anti-human Fas/CD95 (Clone DX2, Biolegend), APC anti-human Nectin-2/CD112 (Clone TX31, Biolegend), APC anti-human PVR/CD155 (Clone SKII.4, Biolegend), PE anti-human MICA (Clone 159227, R&D Systems), PE anti-human MICB (Clone 236511, R&D Systems), PE anti-human ULBP-2/5/6 (Clone 165903, R&D Systems), FITC Mouse IgG1 κ Isotype Control (Clone MOPC-21, Biolegend), APC Mouse IgG1 κ Isotype Control (Clone MOPC-21, Biolegend), and PE Mouse IgG2b κ Isotype Control (Clone MPC-11, Biolegend).

Author contributions

J.S. designed and supervised the study; Y.Z. performed the experiments; Y.Z., J.X. and J.S. analyzed the data; J.S. and Y.Z. wrote the paper.

Acknowledgements

This work was supported by the Hong Kong Research Grant Council (#T12-710/16-R and # C2006-17E) to J. Shi. The authors declare no conflict of interest.

Reference

1. Caligiuri MA. Human natural killer cells. Blood. 2008; 112(3): 461-9.

2. Freud AG, Mundy-Bosse BL, Yu J, Caligiuri MA. The Broad Spectrum of Human Natural Killer Cell Diversity. Immunity. 2017; 47(5): 820-833.

3. Chiossone L, Dumas PY, Vienne M, Vivier E. Natural killer cells and other innate lymphoid cells in cancer. Nat Rev Immunol. 2018; 18(11): 671-688.

4. Ruscetti M, Leibold J, Bott MJ, Fennell M, Kulick A, Salgado NR, Chen CC, Ho YJ, Sanchez-Rivera FJ, Feucht J, Baslan T, Tian S, Chen HA, Romesser PB, Poirier JT, Rudin CM, de Stanchina E, Manchado E, Sherr CJ, Lowe SW. NK cell-mediated cytotoxicity contributes to tumor control by a cytostatic drug combination. Science. 2018; 362(6421): 1416-1422.

5. Souza-Fonseca-Guimaraes F, Cursons J, Huntington ND. The Emergence of Natural Killer Cells as a Major Target in Cancer Immunotherapy. Trends Immunol. 2019; 40(2): 142-158.

6. Lanier LL. NK cell recognition. Annu Rev Immunol. 2005; 23: 225-74.

7. Bryceson YT, March ME, Ljunggren HG, Long EO. Activation, coactivation, and costimulation of resting human natural killer cells. Immunol Rev. 2006; 214: 73-91.

8. Smyth MJ, Swann J, Cretney E, Zerafa N, Yokoyama WM, Hayakawa Y. NKG2D function protects the host from tumor initiation. J Exp Med. 2005; 202(5): 583-8.

9. Champsaur M, Lanier LL. Effect of NKG2D ligand expression on host immune responses. Immunol Rev. 2010; 235(1): 267-85.

10. Cho D, Shook DR, Shimasaki N, Chang YH, Fujisaki H, Campana D. Cytotoxicity of activated natural killer cells against pediatric solid tumors. Clin Cancer Res. 2010; 16(15): 3901-9.

11. Prager I, Watzl C. Mechanisms of natural killer cell-mediated cellular cytotoxicity. J Leukoc Biol. 2019; 105(6): 1319-1329.

12. Smyth MJ, Cretney E, Kelly JM, Westwood JA, Street SE, Yagita H, Takeda K, van Dommelen SL, Degli-Esposti MA, Hayakawa Y. Activation of NK cell cytotoxicity. Mol Immunol. 2005; 42(4): 501-10.

13. Backes CS, Friedmann KS, Mang S, Knörck A, Hoth M, Kummerow C. Natural killer cells induce distinct modes of cancer cell death: Discrimination, quantification, and modulation of apoptosis, necrosis, and mixed forms. J Biol Chem. 2018; 293(42): 16348-16363.

14. Voskoboinik I, Smyth MJ, Trapani JA. Perforin-mediated target-cell death and immune homeostasis. Nat Rev Immunol. 2006; 6(12): 940-52.

15. Bradley M, Zeytun A, Rafi-Janajreh A, Nagarkatti PS, Nagarkatti M. Role of spontaneous and interleukin-2-induced natural killer cell activity in the cytotoxicity and rejection of Fas+ and Fas- tumor cells. Blood. 1998; 92(11): 4248-55.

16. Screpanti V, Wallin RP, Ljunggren HG, Grandien A. A central role for death receptor-mediated apoptosis in the rejection of tumors by NK cells. J Immunol. 2001; 167(4): 2068-73.

17. Gardiner CM, Reen DJ. Differential cytokine regulation of natural killer cell-mediated necrotic and apoptotic cytotoxicity. Immunology. 1998; 93(4): 511-7.

18. Choi PJ, Mitchison TJ. Imaging burst kinetics and spatial coordination during serial killing by single natural killer cells. Proc Natl Acad Sci U S A. 2013; 110(16): 6488-93.

19. Zhu Y, Huang B, Shi J. Fas ligand and lytic granule differentially control cytotoxic dynamics of natural killer cell against cancer target. Oncotarget. 2016; 7(30): 47163-47172.

20. Zhu Y, Zhou Y, Shi J. Post-slippage multinucleation renders cytotoxic variation in anti-mitotic drugs that target the microtubules or mitotic spindle. Cell Cycle. 2014; 13(11): 1756-64.

21. Chan CJ, Smyth MJ, Martinet L. Molecular mechanisms of natural killer cell activation in response to cellular stress. Cell Death Differ. 2014; 21(1): 5-14.

22. Bergert M, Chandradoss SD, Desai RA, Paluch E. Cell mechanics control rapid transitions between blebs and lamellipodia during migration. Proc Natl Acad Sci U S A. 2012; 109(36): 14434-9.

23. Gao Y, Dickerson JB, Guo F, Zheng J, Zheng Y. Rational design and characterization of a Rac GTPase-specific small molecule inhibitor. Proc Natl Acad Sci U S A. 2004; 101(20): 7618-23.

24. Morelli A, Chiozzi P, Chiesa A, Ferrari D, Sanz JM, Falzoni S, Pinton P, Rizzuto R, Olson MF, Di Virgilio F. Extracellular ATP causes ROCK I-dependent bleb formation in P2X7-transfected HEK293 cells. Mol Biol Cell. 2003; 14(**7**): 2655-64.

25. Jänicke RU, Sprengart ML, Wati MR, Porter AG. Caspase-3 is required for DNA fragmentation and morphological changes associated with apoptosis. J Biol Chem. 1998; 273(16): 9357-60.

26. Kazanietz MG, Caloca MJ. The Rac GTPase in Cancer: From Old Concepts to New Paradigms. Cancer Res. 2017;77(20):5445-5451.

27. Cardama GA, Gonzalez N, Maggio J, Menna PL, Gomez DE. Rho GTPases as therapeutic targets in cancer. Int J Oncol. 2017; 51(4): 1025-1034.

28. Olson MF. Rho GTPases, their post-translational modifications, disease-associated mutations and pharmacological inhibitors. Small GTPases. 2018; 9(3): 203-215.

29. Sever R, Brugge JS. Signal transduction in cancer. Cold Spring Harb Perspect Med. 2015; 5(4). pii: a006098.

30. Rak GD, Mace EM, Banerjee PP, Svitkina T, Orange JS. Natural killer cell lytic granule secretion occurs through a pervasive actin network at the immune synapse. PLoS Biol. 2011; 9(9): e1001151.

31. Brown AC, Oddos S, Dobbie IM, Alakoskela JM, Parton RM, Eissmann P, Neil MA, Dunsby C, French PM, Davis I, Davis DM. Remodelling of cortical actin where lytic

granules dock at natural killer cell immune synapses revealed by super-resolution microscopy. PLoS Biol. 2011; 9(9): e1001152.

32. Madjd Z, Spendlove I, Moss R, Bevin S, Pinder SE, Watson NF, Ellis I, Durrant LG. Upregulation of MICA on high-grade invasive operable breast carcinoma. Cancer Immun. 2007; 7: 17.

33. Chen Y, Lin G, Guo ZQ, Zhou ZF, He ZY, Ye YB. Effects of MICA expression on the prognosis of advanced non-small cell lung cancer and the efficacy of CIK therapy. PLoS One. 2013; 8(7): e69044.

34. Li K, Mandai M, Hamanishi J, Matsumura N, Suzuki A, Yagi H, Yamaguchi K, Baba T, Fujii S, Konishi I. Clinical significance of the NKG2D ligands, MICA/B and ULBP2 in ovarian cancer: high expression of ULBP2 is an indicator of poor prognosis. Cancer Immunol Immunother. 2009; 58(5): 641-52.

Figure legend

Figure 1. Characteristics of the cytotoxic dynamics of primary NK cell against five different epithelial cell lines. (A) Cumulative survival curves of target cells, including LO2 (denoted in black), HeLa (green), U-2 OS (blue), SMMC-7721 (magenta) and MCF7 (red), in co-culture with primary human NK cells. (B) Left panels: Fluorescent images of the granzyme-B (GzmB) FRET reporter and the corresponding mitochondria reporter, IMS-RP, from SMMC-7721, U-2 OS and MCF7, respectively. The GzmB-FRET images are overlay of the CFP (denoted by blue) and YFP (denoted by green) channels. Time (unit: hour:minute) is indicated at the top left corner of each GzmB-FRET image. Right panels: Representative single cell trajectories of CFP and YFP signals quantified from the time-lapse movies. The time of MOMP (scored by the IMS-RP signal change) and the time of death (scored morphologically by cell blebbing and lysis) are indicated by the vertical dotted line. (C) Distributions of the live and dead target cells killed by the three distinct cytotoxic modes mediated by lytic granule (with FRET signal loss), death ligand (without FRET signal loss) and necrosis after 12 hours of co-culture with primary NK cells. Data plotted in (A) and (C) were averaged from 2 independent imaging experiments and the number of cells analyzed ranges from 40 to 223, varied between experiments and target cell lines. The error bars are standard deviations.

Figure 2. Surface expressions of the NK cell activating and inhibitory ligands, Fas and ICAM-1 varied between the five target cell lines. (A) Flow cytometry analysis of the surface expressions of the selected proteins by staining with the dye-conjugated antibody specific to the protein (red curves) in comparison with the dye-conjugated, non-specific isotope control (black curves). (B) Comparison of the surface protein expression in the five target cell lines based on the average florescence signal from the flow cytometry analysis. Cell lines were

color coded as indicated. Data were averaged from 2 independent flow cytometry analyses (>1×10^4 cells in each analysis). The error bars are standard deviations.

Figure 3. Neutralizing the inhibitory and activating receptors of primary NK cells showed differential effect on altering the cell death response of the five target cell lines. (A) Cumulative survival curves of HeLa cells in co-culture with primary NK cells in the presence of single or double blockage of the inhibitory receptor (left panel) or activating receptor (right panel). (B) Distributions of live and dead HeLa cells killed by the three distinct cytotoxic modes after 12 hours of co-culture with NK cells under the indicated treatment conditions. (C) Percentage of live cells (upper left panel) and cells that died via the three cytotoxic modes under the different receptor blocking conditions in comparison with those under the control condition. Data from the five target cell lines were color coded as LO2 in black, HeLa in green, U-2 OS in blue, SMMC-7221 in magenta and MCF7 in red. The different treatment conditions were denoted with the indicated symbols. Data plotted were averaged from 2 or 3 independent imaging experiments and the error bars are standard deviations.

Figure 4. Membrane dynamics alter NK cell cytotoxic modes against different epithelial target cell lines. (A) Left panel: Phase-contrast images of MCF7, SMMC-7721 and U-2 OS cells under control or treatment of NSC23766 (Rac inhibitor) or Y27632 (ROCK inhibitor). Right-panel: Kymograph of the cell edge of MCF7, SMMC-7721 and U-2 OS cells under the indicated treatment conditions. (B, C) Distributions of the four response phenotypes of target cells under control or the indicated inhibitor treatment for (B) MCF7 cells or (C) SMMC-7721 cells in co-culture with primary NK cells for 12 hours. (D) Phase-contrast images and the response phenotype distribution of SMMC-7721 cells that adhered to the cell culture plate for 4 hours (with or without Y27632) and in co-cultured with primary NK cells for 12 hours in comparison with control cells that adhered for 24 hours. (E) Left panel:

cumulative survival curves of MCF7 cells in co-culture with primary NK cells under the control condition or in the presence of 10 nM Concanamycin A (CMA). Right panel: distribution of the indicated response phenotypes of MCF7 cells after 12-hour co-culture with primary NK cells as a function of CMA concentration. Data plotted in (A) to (E) were averaged from 2 to 4 independent imaging experiments and the number of cells analyzed for each condition/cell line ranges from 44 to 149. The error bars are standard deviations. P value was obtained by student's t test comparing the treatment condition with control. * $P < 0.001$.

Figure 1

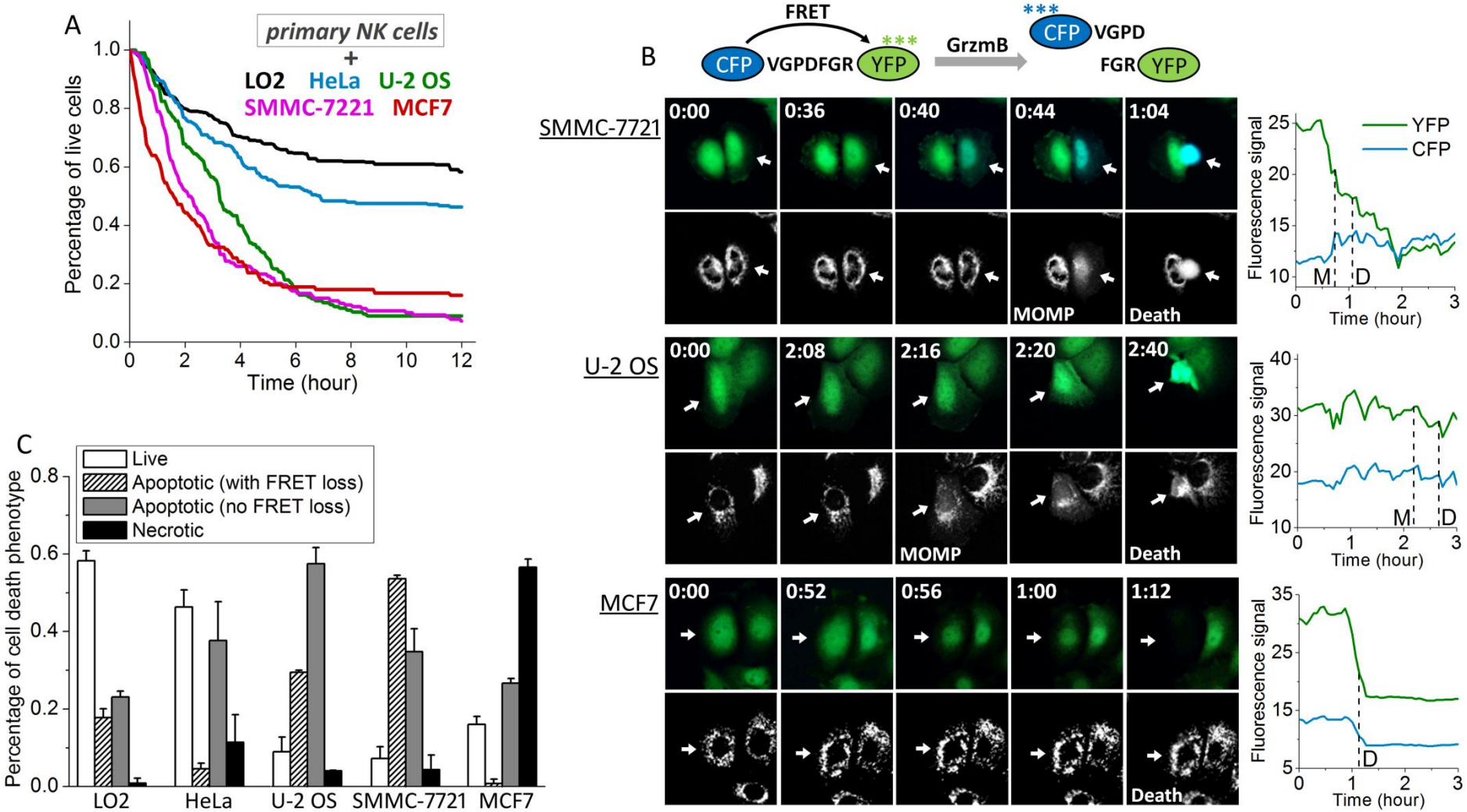
A
primary NK cells
+
LO2 HeLa U-2 OS
SMMC-7221 MCF7
Percentage of live cells
Time (hour)
B
FRET
CFP VGPDFGR YFP
GrzmB
CFP VGPD
FGR YFP
SMMC-7721
0:00 0:36 0:40 0:44 1:04
MOMP
Death
YFP
CFP
Fluorescence signal
M D
Time (hour)
U-2 OS
0:00 2:08 2:16 2:20 2:40
MOMP
Death
MCF7
0:00 0:52 0:56 1:00 1:12
Death
C
Live
Apoptotic (with FRET loss)
Apoptotic (no FRET loss)
Necrotic
Percentage of cell death phenotype
LO2 HeLa U-2 OS SMMC-7721 MCF7

Figure 2

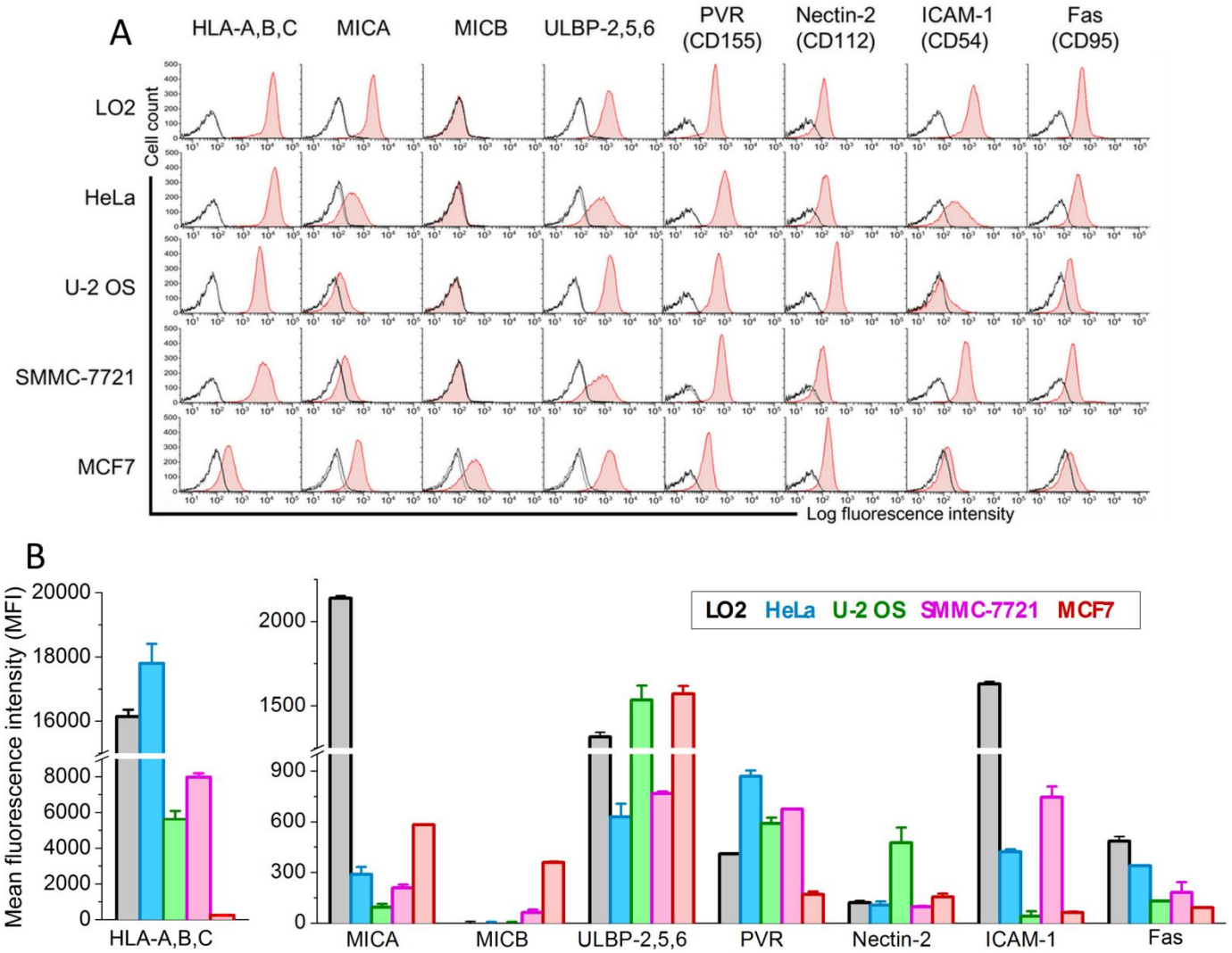
A
HLA-A,B,C
MICA
MICB
ULBP-2,5,6
PVR (CD155)
Nectin-2 (CD112)
ICAM-1 (CD54)
Fas (CD95)
LO2
HeLa
U-2 OS
SMMC-7721
MCF7
Cell count
Log fluorescence intensity
B
Mean fluorescence intensity (MFI)
LO2 HeLa U-2 OS SMMC-7721 MCF7
HLA-A,B,C
MICA
MICB
ULBP-2,5,6
PVR
Nectin-2
ICAM-1
Fas

Figure 3

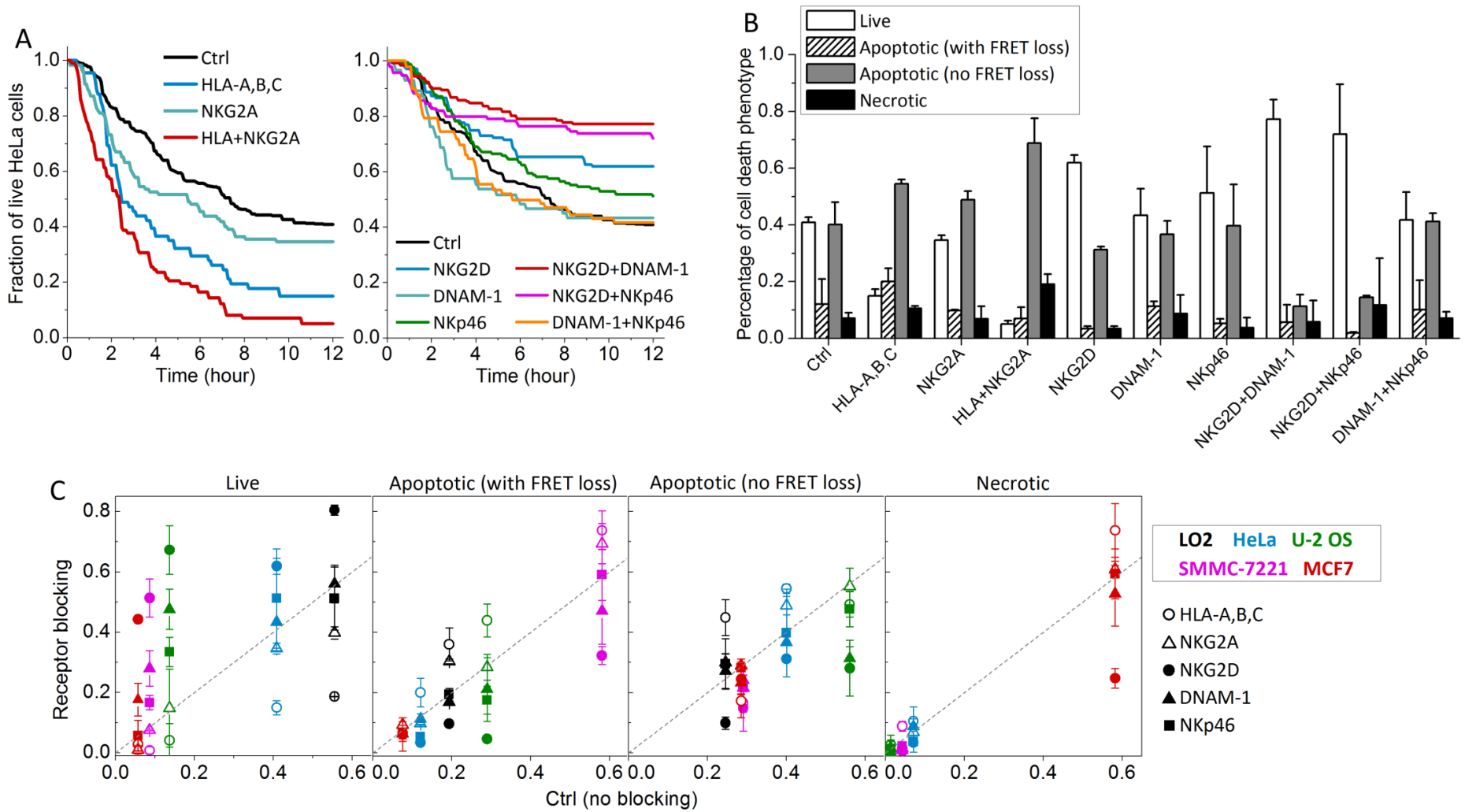
A
Fraction of live HeLa cells
Time (hour)
Ctrl
HLA-A,B,C
NKG2A
HLA+NKG2A
NKG2D
DNAM-1
NKp46
NKG2D+DNAM-1
NKG2D+NKp46
DNAM-1+NKp46
B
Percentage of cell death phenotype
Live
Apoptotic (with FRET loss)
Apoptotic (no FRET loss)
Necrotic
Ctrl
HLA-A,B,C
NKG2A
HLA+NKG2A
NKG2D
DNAM-1
NKp46
NKG2D+DNAM-1
NKG2D+NKp46
DNAM-1+NKp46
C
Live
Apoptotic (with FRET loss)
Apoptotic (no FRET loss)
Necrotic
Receptor blocking
Ctrl (no blocking)
LO2
HeLa
U-2 OS
SMMC-7221
MCF7
HLA-A,B,C
NKG2A
NKG2D
DNAM-1
NKp46

Figure 4

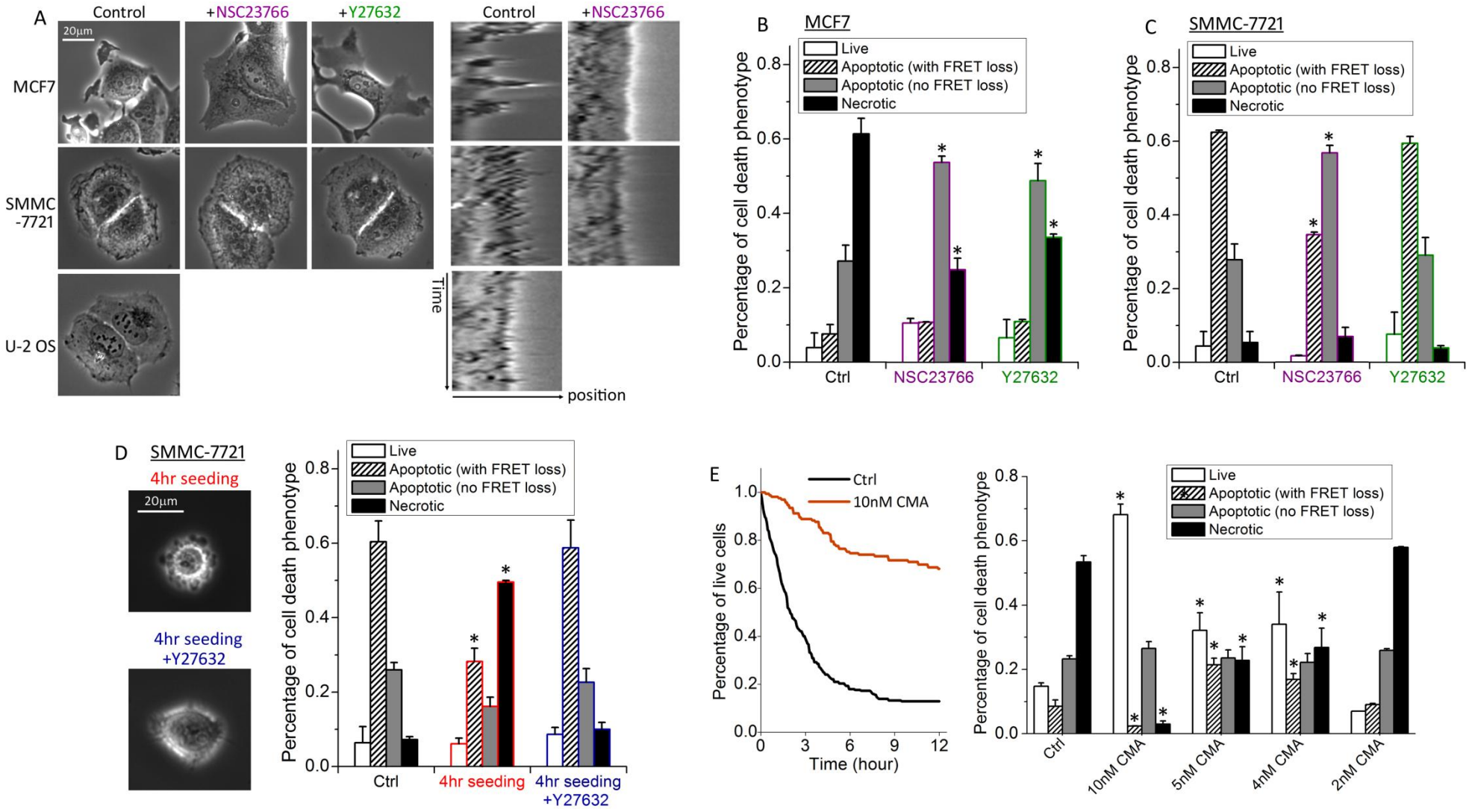
A
Control
+NSC23766
+Y27632
Control
+NSC23766
20μm
MCF7
SMMC -7721
U-2 OS
Time
position
B
MCF7
Live
Apoptotic (with FRET loss)
Apoptotic (no FRET loss)
Necrotic
Percentage of cell death phenotype
Ctrl
NSC23766
Y27632
C
SMMC-7721
Live
Apoptotic (with FRET loss)
Apoptotic (no FRET loss)
Necrotic
Percentage of cell death phenotype
Ctrl
NSC23766
Y27632
D
SMMC-7721
4hr seeding
20μm
4hr seeding +Y27632
Live
Apoptotic (with FRET loss)
Apoptotic (no FRET loss)
Necrotic
Percentage of cell death phenotype
Ctrl
4hr seeding
4hr seeding +Y27632
E
Ctrl
10nM CMA
Percentage of live cells
Time (hour)
Live
Apoptotic (with FRET loss)
Apoptotic (no FRET loss)
Necrotic
Percentage of cell death phenotype
Ctrl
10nM CMA
5nM CMA
4nM CMA
2nM CMA